JTTEE5 14:251-257
DOI: 10.1361/10599630523827
1059-9630/$19.00 © ASM International

Improvement of Wear Resistance of Plasma-Sprayed Molybdenum Blend Coatings

Jeehoon Ahn, Byoungchul Hwang, and Sunghak Lee

(Submitted November 4, 2003; in revised form February 23, 2004)

The wear resistance of plasma sprayed molybdenum blend coatings applicable to synchronizer rings or piston rings was investigated in this study. Four spray powders, one of which was pure molybdenum and the others blended powders of bronze and aluminum-silicon alloy powders mixed with molybdenum powders, were sprayed on a low-carbon steel substrate by atmospheric plasma spraying. Microstructural analysis of the coatings showed that the phases formed during spraying were relatively homogeneously distributed in the molybdenum matrix. The wear test results revealed that the wear rate of all the coatings increased with increasing wear load and that the blended coatings exhibited better wear resistance than the pure molybdenum coating, although the hardness was lower. In the pure molybdenum coatings, splats were readily fractured, or cracks were initiated between splats under high wear loads, thereby leading to the decrease in wear resistance. On the other hand, the molybdenum coating blended with bronze and aluminum-silicon alloy powders exhibited excellent wear resistance because hard phases such as $CuAl_2$ and Cu_9Al_4 formed inside the coating.

Keywords atmospheric plasma spraying, hardness, molybdenum blend coating, wear resistance

1. Introduction

Among thermal spraying methods, plasma spraying is most widely applied in the automotive industries (Ref 1-3) because (a) it has a high spray rate and deposition, (b) the process consumes fuel gases which are inexpensive and easily obtainable, (c) the process requires minimum preheating and cooling during spraying, (d) the technical reliability of plasma systems is well established in industrial applications, and (e) spraying conditions can be easily controlled upon various applications (Ref 4). In particular, molybdenum coatings fabricated by atmospheric plasma spraying have enhanced resistance to wear and heat (Ref 5-11), and thus this coating technology was commercialized for application to the automotive industry. However, the coatings often pose problems of embrittlement caused by high hardness, despite their excellent high-temperature hardness and corrosion resistance, when applied to automotive parts such as cylinder bores (Ref 1, 12), synchronizer rings (Ref 9-11), and piston rings (Ref 9). These applications require excellent wear resistance of both the coating and the counterpart material. To overcome these shortcomings and to improve overall wear resistance, studies on molybdenum coatings have focused on enhancing overall wear resistance by blending powders such as NiCrBSi, brass, bronze, and Mo_2C powders with molybdenum powders (Ref 5, 8-11).

In this study, a pure Mo coating and three Mo blended coatings were fabricated by atmospheric plasma spraying. The effects of coating microstructure on hardness and wear resistance as a function of wear load were investigated.

Jeehoon Ahn, Byoungchul Hwang, and **Sunghak Lee,** Center for Advanced Aerospace Materials, Pohang University of Science and Technology, Pohang 790-784, Korea. Contact e-mail: shlee@postech.ac.kr.

2. Experimental

Three powders, pure Mo, Al-Si alloy (Al-12%Si), and bronze powders, were used to fabricate the Mo blended coatings, and detailed powder characteristics are shown in Table 1. The particle sizes of bronze and Al-Si powders are confined in the range from 45-90 μm to obtain high-density coatings by increasing flowability of powders inside the plasma jet stream. Mo powders exhibit an irregular morphology because they are processed by a sintering and crushing process. The bronze powders processed by water atomization have an irregular shape, while Al-Si powders processed by gas atomization are fine and spheroidal.

One of the Mo coatings was fabricated with pure Mo powders, and three of the Mo blended coatings were fabricated by mixing Mo powder with bronze and Al-Si powders using a turbulent shake mixer. For convenience, the Mo coating fabricated with pure Mo powders is referred to as A, the blended coatings fabricated with pure Mo + 50 wt.% bronze powders and pure Mo + 50 wt.% Al-Si powders as B and C, respectively, and the blended coating fabricated with pure Mo + 25 wt.% bronze + 25 wt.% Al-Si powders as D.

A plain carbon steel [chemical composition: Fe-0.45C-0.3Si-0.75Mo-0.03P-0.035S (wt.%)] was used as a substrate. Its surface was polished and blasted with Al_2O_3 grit to improve the adhesive coating/substrate bonding strength, and this was ultrasonically cleansed.

Plasma spraying on the substrate was conducted using a Sulzer Metco 9MB spray system (Westbury, NY), and argon combined with hydrogen was used as the plasma gas. A specimen holder was cooled with compressed air to prevent overheating during the spray process. Plasma spray conditions were fixed at the optimal parameters (arc flow rate, 80 l/min; arc pressure, 0.69 MPa; auxiliary gas flow rate, 10 l/min; auxiliary gas pres-

Table 1 Compositions and characteristics of powders used for atmospheric plasma spray coating

Powder	Composition	Particle size, μm	Particle shape	Manufacturing method	Manufacture company and brand name
Mo	Mo 99%	45~75	Irregular	Sintered & crushed	Sulzer Metco Inc. "Metco 63NS"
Bronze	Cu-10%Sn	45~90	Irregular	Water atomized	Fukuda Metal Foil & Powder Co. "Bro-Atw-200"
Al-12Si	Al-12%Si	45~90	Spheroidal	Gas atomized	Sulzer Metco Inc. "Metco 52C-NS"

sure, 0.345 MPa; spray rate, 3.81 kg/h; arc voltage, 66 V; arc current, 500 Amp; and spray distance, 98 mm). Surface roughness of the coatings was measured by a roughness gage (Model; Surfest 402, Mitutoyo Co., Kawasaki, Japan), and thickness of the coatings was measured by observing the sectioned areas of the coatings using a low-magnification optical microscope. The coatings were sectioned perpendicular to the coated surface, and their microstructures were observed by an optical microscope and a scanning electron microscope (SEM; JSM-6330F, JEOL, Tokyo, Japan). Phases present in the coatings and their chemical compositions were analyzed by x-ray diffraction (XRD) (D/max 2500H, Rigaku, Tokyo, Japan) and energy dispersive spectroscopy (EDS; INCA Energy, Oxford, U.K.) analyses. Hardness was measured by a Vickers hardness tester (DMH-2, Durban, South Africa) under a 300 g load, and microhardness of matrix and phases was measured under a 10 g load with an ultra-micro-Vickers hardness tester (DUH-200, Shimadzu, Tokyo, Japan).

Wear testing was conducted on the coatings using a pin-on-disk type wear tester (EFM-III-EN/F, Orientec Co., Tokyo, Japan) in accordance with ASTM G99-95a specification (Ref 13). An SCM420 steel [chemical composition: Fe-0.2C-0.2Si-0.7Mn-1.0Cr-0.2Mo (wt.%)] was used for the pin (counterpart material) of 5 mm in diameter. The pin was surface-hardened to 700 VHN by a carbonizing treatment to match the hardness level of a commercial cone ring used as a counterpart component of a synchronizer ring.

The coatings were sectioned to 30 × 30 mm and ground to make the surface roughness constant at about 0.1 μm. The coated disk specimen was worn in contact with the upper pin under loads of 5, 10, and 20 kgf at 100 °C for 30 min. An SAE 80W90 gear oil (Petro Canada, Calgary, Canada) was used as a lubricant. Wear track radius, rotation speed, and wear distance were 12 mm, 200 rpm, and 450 m, respectively. Volume loss of the coated disk specimen was obtained by the standard method in accordance with ASTM G99-95a specification (Ref 13), and this value was converted to wear rate (unit: mm^3/m). After the test, the worn surface and cross-sectional area of the disk specimen were observed by SEM.

3. Results and Discussion

3.1 Microstructure

Optical micrographs of the coatings are shown in Fig. 1(a)-(d). Elongated splats, which are typical of spray coatings, are formed, and pullouts of splats occurred during polishing are also found (Ref 4, 14). The phases are relatively homogeneously distributed in the matrix of the blended coatings (the B through D specimens). Unmelted particles are not observed in the coatings due to complete melting during spraying. There are no reaction products at the coating/substrate interfaces, which indicates good bonding between them. The thickness and surface roughness (Ra) of the coatings were measured, and the results are shown in Table 2. The thickness of the coatings ranges from 300 to 550 μm, and the surface roughness (Ra) ranges from 11 to 15 μm.

Figures 2(a)-(c) show SEM micrographs of the blended coatings. The C and D specimens exhibit relatively stable bonding at interfaces between matrix and blended phases, but the B specimen has a poor microstructure where a number of pores exist inside the coating and interfaces between splats are unstable (Fig. 2a). The B and C specimens consist of two regions (Fig. 2a and b), while the D specimen consists of four regions (Fig. 2c). These regions were analyzed by EDS. Mo was detected in the matrix (white region) of the B and C specimens, while Cu and Sn, and Al and Si were detected in the gray regions of the B and C specimens, respectively. In the D specimen, four regions are observed Fig. 2(c). Mo, Cu, and Al are detected in the white matrix region, light gray region, and dark gray region, respectively. Cu and Al are simultaneously detected at interfaces between the light gray and dark gray regions.

Figure 3 shows XRD analysis results of the coatings. In the A specimen, only Mo is detected, while α(Cu-Sn) and Al(-Si) are additionally detected besides Mo in the B and C specimens, respectively. In the D specimen, not only all the phases detected in the B and C specimens are present, but new phases such as $CuAl_2$ and Cu_9Al_4 are also observed. Since the powders used in this study do not react with oxygen in the air during spraying, oxides are not detected in all the coatings. Phases identified by XRD and EDS analyses are marked in Fig. 2(a)-(c).

3.2 Hardness

The bulk hardness and microhardness of the blended phases contained inside the coatings are shown in Table 2. The bulk hardness is highest in the A specimen and decreases in the order of the D, C, and B specimens, depending on the type of blended phases. In all the specimens, the matrix hardness ranges from 450 to 490 VHN, and the hardness of the bronze and Al-Si regions in the B and C specimens are 212 and 153 VHN, respectively. The hardness of the blended phases in the D specimen was from 223, 138, and 706, depending on the regions of Fig. 2(c). The B through D specimens exhibit lower overall bulk hardness values than the A specimen due to the low hardness of the blended phases. The overall bulk hardness of the B specimen is slightly lower than that of the C specimen, although the hardness of the blended phases is higher than that of the C specimen. This behavior might be associated with the less-densified coating in the B specimen due to the presence of numerous pores and unstable splats as shown in Fig. 2(a). Thus, the hardness of the coatings is affected by the hardness of the matrix and blended phases, volume fraction of blended phases, and porosity.

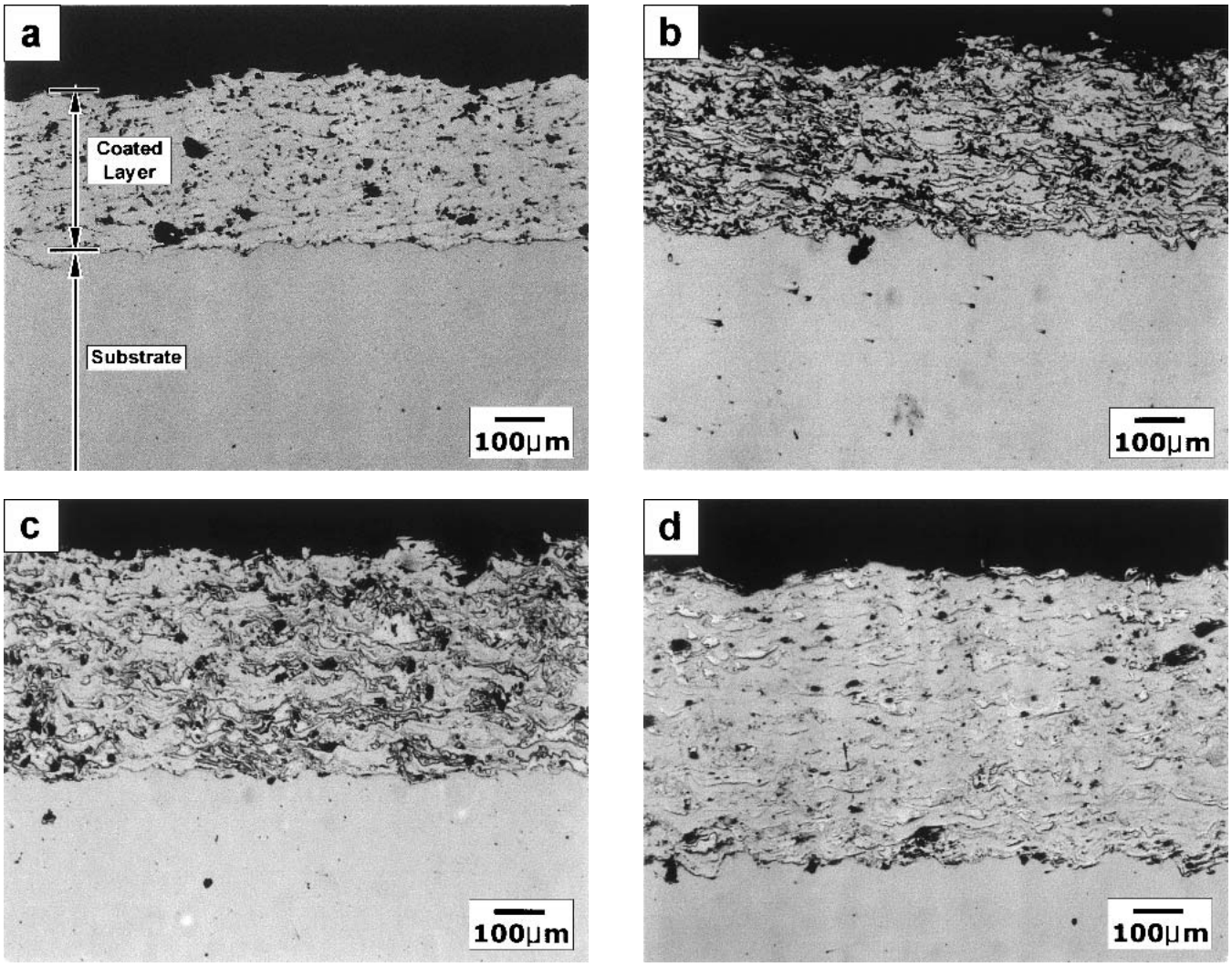

Fig. 1 Optical micrographs of the (a) A, (b) B, (c) C, and (d) D specimens; not etched

Table 2 Properties of the molybdenum blended coatings

Specimen	Thickness, µm	Roughness, Ra, µm	Vickers hardness VHN		
			Matrix(a)	Blended phase(a)	Overall bulk(b)
A	297 ± 14	11.5 ± 2.3	467 ± 36	…	342 ± 39
B	338 ± 16	11.3 ± 1.8	457 ± 32	212 ± 15	137 ± 23
C	416 ± 23	14.5 ± 3.1	472 ± 26	153 ± 24	157 ± 48
D	558 ± 20	15.4 ± 3.3	489 ± 47	223 ± 63 (Cu-Sn) 138 ± 35 (Al-Si) 706 ± 89 (Cu-Al)	224 ± 25

(a) Vickers microhardness values measured under a load of 10 g. (b) Vickers microhardness values measured under a load of 300 g

3.3 Wear Resistance

The pin-on-disk wear test results are shown in Fig. 4. The wear rate of the coatings rises with increasing the wear load. The Mo blended coatings show a wear rate of less than 1/2-1/5 of the pure Mo coating. Though the wear rate is about the same under a load of 5 kgf, it further varies when the wear load increases. Under a 20 kgf load, the wear rate decreases in the order of the A, B, C, and D specimens.

Three kinds of the Mo blend coatings demonstrate more excellent wear resistance than the pure Mo coating under all wear load conditions. Although the pure Mo coating shows higher hardness than the Mo blended coatings, it has a higher wear rate than the other materials. The higher wear rate arises because wear in the Mo and Mo blended coatings depends on factors such as microstructure and wear load. In general, hardness is the most critical factor affecting wear resistance. However, internal factors such as ductility, presence of pores and cracks inside

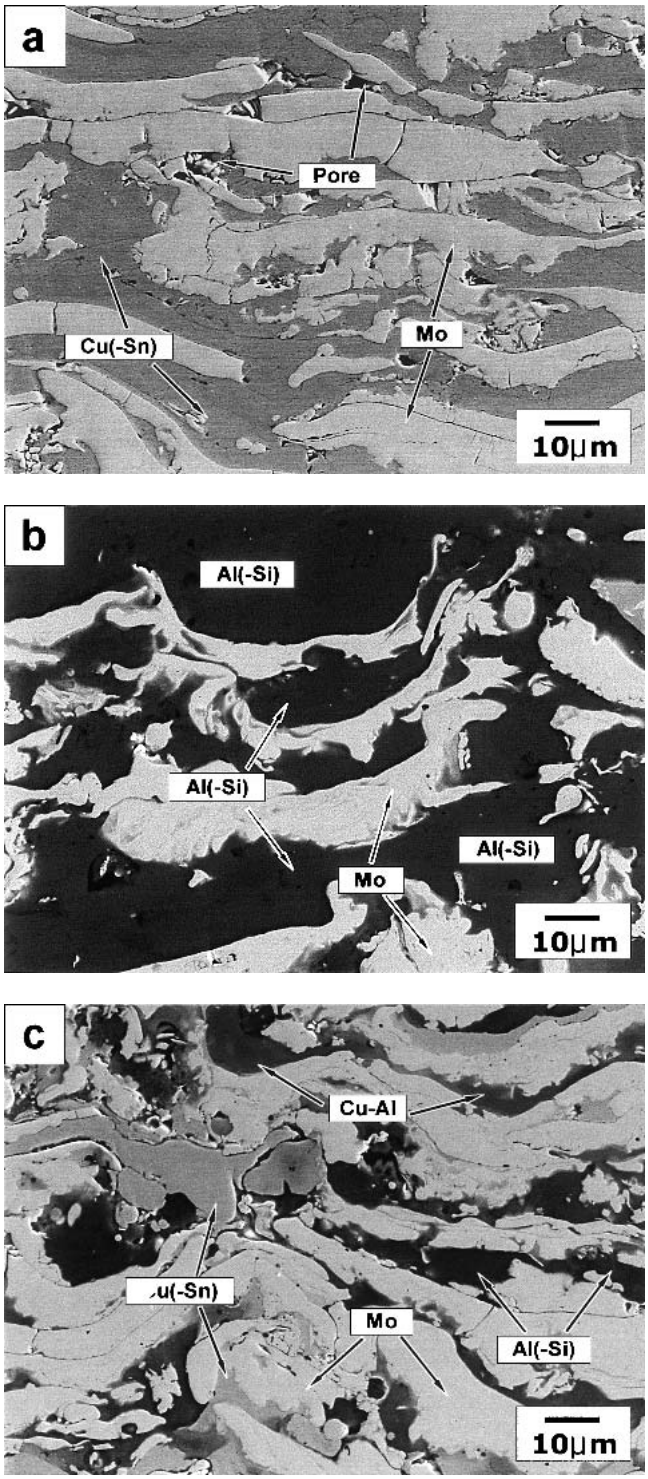

Fig. 2 SEM micrographs of the (a) B, (b) C, and (c) D specimens; not etched

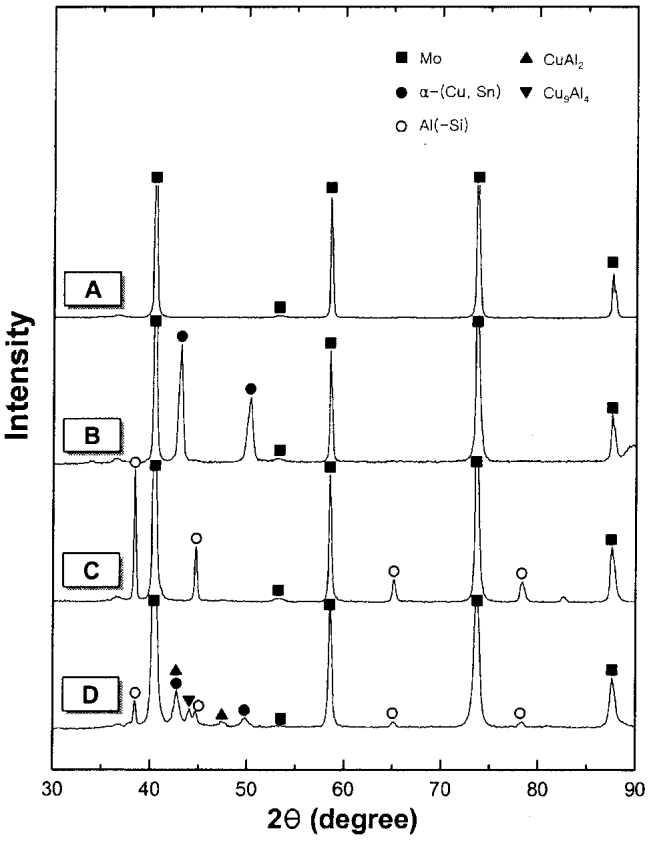

Fig. 3 X-ray diffraction patterns of the coatings

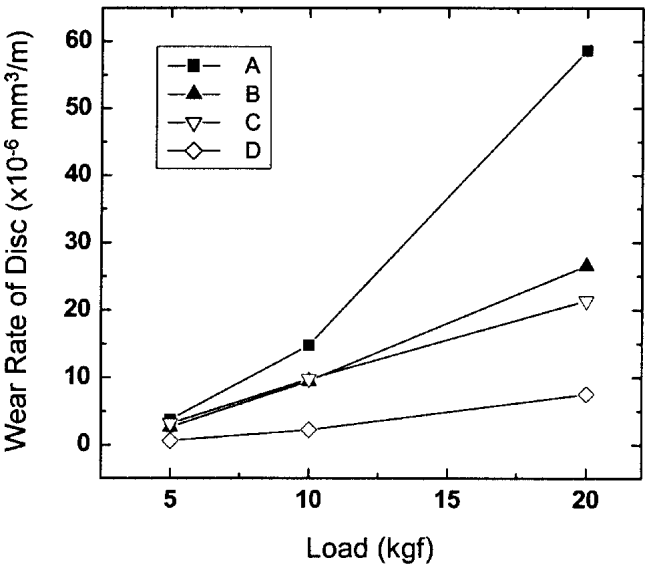

Fig. 4 Variation of wear rate of the coatings as a function of wear load

coatings, and shape, morphology, and distribution of blended phases as well as external factors including load, speed, distance, counterpart material, dry- and wet-mixing condition, and temperature do play important roles in wear process (Ref 15-17). To analyze the wear resistance of the Mo and Mo blended coatings, worn surfaces and cross-sectional areas of the coatings were observed.

Figures 5(a)-(d) are SEM micrographs of the coating surfaces worn under a load of 20 kgf. The worn surfaces of all the specimens show a typical abrasive wear mode in which grooves are

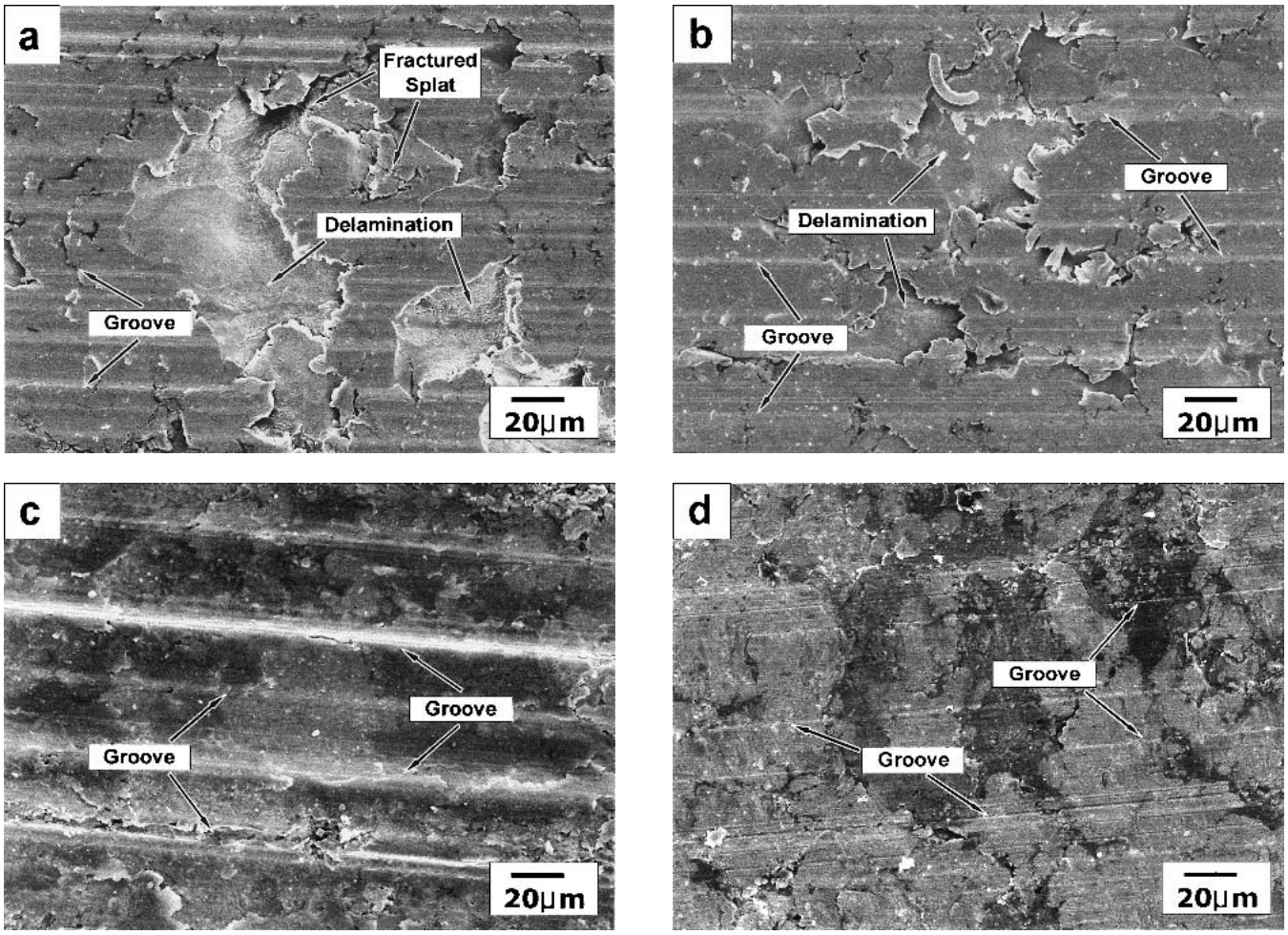

Fig. 5 SEM micrographs of the worn surface of the (a) A, (b) B, (c) C, and (d) D specimens after the wear test under a load of 20 kgf

formed along the wear direction, and some microcracks are found. On the worn surfaces of the A and B specimens, regions where parts of the coating have delaminated are clearly visible together with grooves (arrow marks in Fig. 5a and b). The grooves are deep in the C specimen due to the lowest hardness, whereas they are shallow and almost unnoticeable in the D specimen (arrow marks in Fig. 5c and d).

The worn cross-sectional areas were observed by SEM, as shown in Fig. 6(a)-(d). In the A specimen, areas formed when splats near the worn surface were either fractured or delaminated are observed, as indicated by arrows in Fig. 6(a). In the B specimen, areas where splats near the worn surface are separated and fallen off are observed, as in the A specimen (Fig. 6b). The worn surfaces of the C and D specimens are relatively smooth, and microcracks are rarely found beneath the worn surfaces.

The worn surface and cross-sectional area of the A specimen (Fig. 5a and 6a) reveal that the Mo coating composed of Mo splats only is brittle due to the high hardness of splats. Thus, interfaces between splats can be easily separated, or some splats are fractured (Ref 5). Such phenomena of fracture and delamination vary with wear load and considerably affect the wear rate. Since fracture and delamination become more severe as the wear load increases from 10 to 20 kgf, the wear rate is accelerated, thereby leading to the transition of wear mechanisms.

Liu et al. (Ref 7) reported that hard phases were cracked and fractured in Mo coatings fabricated by flame spraying when the wear load increased and that three steps of wear and a transition of wear mechanisms from mild wear to severe one were observed. Likewise, in the case of other coatings fabricated by plasma spraying, it is known that the wear mechanism changes with the wear load (Ref 12, 17). In the B specimen, splats near the worn surface readily fall off along the interfaces due to the poor microstructure of the coating itself, and then the wear transition takes place as in the A specimen. Thus, the B specimen shows much higher wear rate than other Mo blended coatings. In the C specimen, the wear rate is slower than in the B specimen because splats near the worn surface are do not fall off easily since there is good interfacial contact between the matrix and blended phases under high wear loads.

In the D specimen, new phases, which were not present in the B and C specimens, are found. As shown in Fig. 2(c), blended regions where both Al and Cu are detected are confirmed to be $CuAl_2$ and Cu_9Al_4 from the x-ray diffraction data (Fig. 3). These phases seem to have been formed when bronze and Al-Si powders were coalesced during melting and spraying by high-

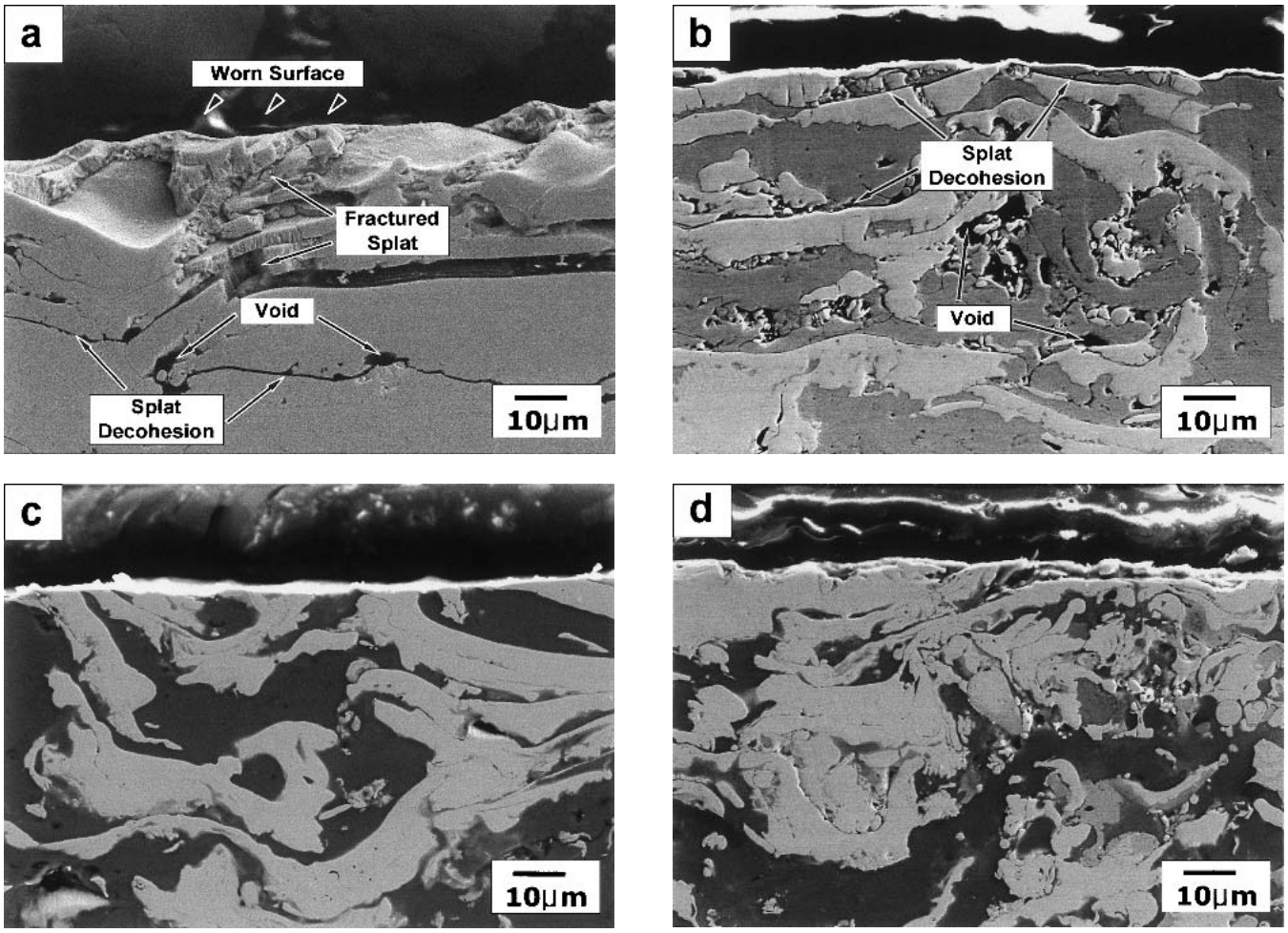

Fig. 6 SEM micrographs of the cross-sectional area of the (a) A, (b) B, (c) C, and (d) D specimens after the wear test under a load of 20 kgf

temperature plasma, were deposited on the substrate, and went through the aging process of a supersaturated solid solution while maintained at a stable temperature (Ref 18-20). Al-Cu alloy is a typical age-hardened one whose major hardening phases are metastable θ′($CuAl_2$) (Ref 20-23). Since phases formed in Al-Cu alloys such as $CuAl_2$, Cu_9Al_4, and CuAl have extremely high hardness (Ref 20), the D specimen shows higher overall bulk hardness than other Mo blended coating specimens (Table 2). According to Fig. 2(c), splats are comparatively smaller than those of other Mo blended coatings, since $CuAl_2$ and Cu_9Al_4 phases are relatively homogeneously distributed throughout the coating. These hard phases increase wear resistance as well as overall bulk hardness of the coating (Fig. 4 and Table 2). Their susceptibility to fracture or delamination during the wear process is low, and thus there is a larger amount of abrasive material against the counterpart material. Therefore, the wear resistance of the D specimen is excellent in consideration of the wear resistance of the coating.

4. Conclusions

This study has presented several wear-resistant Mo blended coatings for application to synchronizer rings or piston rings. Major factors that affect the wear rate of the coating concern the relationship between the microstructure and wear load. The primary conclusions are as follows:

- The Mo blended coatings showed lower hardness than the pure Mo coating, but the wear rate of the blended coatings were significantly lower than that of the pure Mo coating.
- In the pure Mo coating, splats were fractured under high wear loads, or cracks were initiated between splats due to their brittleness, thereby leading to delamination of the coating. Thus, the wear rate was higher than that of the Mo blended coatings.
- In the Mo blended coating where bronze and Al-Si powders were used, hard $CuAl_2$ and Cu_9Al_4 phases formed while the two powders were melted and deposited on the substrate during spraying, together with other hard phases. The hard phases contributed to excellent wear resistance of this coating.

References

1. V.D.N. Rao, D.M. Kabat, H.A. Cikanek, C.A. Fucinari, and G. Wuest, Material Systems for Cylinder Bore Applications—Plasma Spray Technology, *SAE Paper,* No. 970023, 1997, p 107-132

2. G. Barbezat and G. Wuest, Advantages for Automotive Industry of Plasma Spray Coating of Al-Si Cast Alloy Cylinder Bores, *Surf. Eng.,* Vol 14, 1998, p 113-116
3. Th. Lampe, S. Eisenberg, and E.R. Cabeo, Plasma Surface Engineering in the Automotive Industry-Trends and Future Prospectives, *Surf. Coat. Technol.,* Vol 174-175, 2003, p 1-7
4. L. Pawlowski, *The Science and Engineering of Thermal Spray Coatings,* John Wiley & Sons, New York, 1995
5. S.F. Wayne, S. Sampath, and V. Anand, Wear Mechanisms in Thermally-Sprayed Mo-Based Coatings, *Tribol. Trans.,* Vol 37 (No. 3), 1994, p 636-640
6. Y.S. Kim, Influences of Alloyed Molybdenum and Molybdate Addition on the Corrosion Properties and Passive Film Composition of Stainless Steels, *Metall. Mater. Intern.,* Vol 4, 1998, p 183-191
7. Z. Liu and M. Hua, Wear Transitions and Mechanisms in Lubricated Sliding of a Molybdenum Coating, *Tribol. Intern.,* Vol. 32, 1999, p 499-506
8. B. Hwang, S. Lee, and J. Ahn, Correlation of Microstructure and Wear Resistance of Molybdenum and Molybdenum Blend Coatings Fabricated by Atmospheric Plasma Spraying, *Mater. Sci. Ena.,* Vol A366, 2004, p 152-163
9. S. Sampath, S. Usmani, and D.L. Houck, Applications of Mo and Mo-Alloys as Thermal Spray Coatings, in *Molybdenum and Molybdenum Alloys,* A. Crowson, E.S. Chen, J.A. Shields, and P.R. Subramanian, Ed., TMS, 1998, p 415-424
10. J.M. Tura, A. Traveria, M.D. de Castellar, J. Pujadas, J. Blouet, R. Gras, H.G. Magham, P. Belair, T. Hanau, and A. Romero, Frictional Properties and Wear of a Molybdenum Coating and a Bronze (Cu-10%Sn) with Friction Modifier Fillers, *Wear,* Vol 189, 1995, p 70-76
11. K. Nakashima, M. Hosoda, W. Yago, and K. Inagaki, Synchronizer Ring Having a Spray-Coated Film of a Wear-Resistant Brass Material, US Patent 5 326 646, July 1994
12. B. Hwang, J. Ahn, and S. Lee, Correlation of Microstructure and Wear Resistance of Ferrous Coatings Fabricated by Atmospheric Plasma Spraying, *Metall. Mater. Trans. A,* Vol 33A, 2002, p 2933-2945
13. ASTM G99-95a, ASTM Standard Test Method for Wear Testing with a Pin-on-Disk Apparatus, ASTM, Philadelphia, 1995, p 1-5
14. S. Sampath and H. Herman, Rapid Solidification and Microstructure Development during Plasma Spray Deposition, *J. Therm. Spray Technol.,* Vol 5, 1996, p 445-456
15. S-H. Kim and Y-S. Kim, Effect of Ductility on Dry Sliding Wear of Medium Carbon Steel under Low Load Condition, *Met. Mater. Int.,* Vol 5, 1999, p 267-271
16. D.A. Rigney, *Fundamentals of Friction and Wear of Materials,* ASM, Materials Park, OH, 1981
17. M. Gui and S.B. Kang, Dry Sliding Wear Behavior of Plasma-Sprayed Aluminum Hybrid Composite Coating, *Metall. Mater. Trans. A,* Vol 32A, 2001, p 2383-2392
18. D.A. Porter and K.E. Easterling, *Phase Transformation in Metals and Alloys,* Chapman & Hall, London, 1992
19. K.T. Conlon, E. Maire, D.S. Wilkinson, and H. Henein, Processing and Microstructural Characterization of Al-Cu Alloys Produced from Rapidly Solidified Powders, *Metall. Mater. Trans. A,* Vol 31A, 2000, p 249-260
20. D. Moreno, J. Garrett, and J.D. Embury, A Technique for Rapid Characterization of Intermetallics and Interfaces, *Intermetallics,* Vol 7, 1999, p 1001-1009
21. Z. Shi, A. Bloyce, Y. Sun, and T. Bell, Influence of Surface Melting on Dry Rolling-Sliding Wear of Aluminum Bronze against Steel, *Wear,* Vol 198, 1996, p 300-306
22. S. Tomida, K. Nakata, S. Saji, and T. Kubo, Formation of Metal Matrix Composite Layer on Aluminum Alloy with TiC-Cu Powder by Laser Surface Alloying Process, *Surf. Coat. Tech.,* Vol 142, 2001, p 585-589
23. S. Alam, S. Sasaki, and H. Shimura, Friction and Wear Characteristics of Aluminum Bronze Coatings on Steel Substrates Sprayed by a Low Pressure Plasma Technique, *Wear,* Vol 248, 2001, p 75-81